Acta of Bioengineering and Biomechanics
Vol. 24, No. 2, 2022

Original paper
DOI: 10.37190/ABB-02065-2022-02

Kinematic analysis of L4–L5 spinal segment with spondylolysis and different types of grade 1 spondylolisthesis: a nonlinear finite element study

SUHAIB YAROUB[1]*, SADIQ J. HAMANDI[1], KHALEEL MOHSON[2]

[1] Department of Biomedical Engineering, College of Engineering, Al-Nahrain University, Jadriya, Baghdad, Iraq.
[2] Iraqi National Cancer Research Center, University of Baghdad, Baghdad, Iraq.

Purpose: This work aimed to evaluate and characterize the motion of the fourth and fifth lumbar vertebrae functional spinal unit with spondylolysis and different types of grade 1 spondylolisthesis using the finite element method. *Methods*: Nine nonlinear three-dimensional finite element models were reconstructed from computed tomography scans to five educational fourth and fifth lumbar vertebrae models. The intervertebral disc was simulated in two conditions: four models with healthy discs and five models with degenerated discs. Each model consisted of two vertebrae divided into three bony parts, two endplates, an intervertebral disc and five ligaments. The flexion, extension, lateral bending and rotation loading conditions were simulated, and the ranges of motion were measured and plotted. *Results*: In flexion, compared to the baseline intact model, the most significant increase in the range of motion was experienced by the isthmic spondylolisthesis model, while in extension, a reduction in the range of motion was measured in both prolonged pars and unilateral pars defect and healthy disc models. In degenerated disc results, the unilateral pars defect and degenerative spondylolisthesis models had the lowest range of motion. No large differences were noticed in lateral bending results. Lastly, in axial rotation, the most significant increase in the range of motion was measured in the isthmic spondylolisthesis model, followed by the spondylolysis model and similarly, in the degenerated disc models. *Conclusions*: The isthmic spondylolisthesis displayed hypermobility in flexion and rotation. Moreover, the model with unilateral pars defect showed hypermobility in axial rotation only. Finally, hypomobility in all movements was noticed with the degenerative spondylolisthesis model.

Key words: *kinematics, finite element analysis, lumbar spine, spondylolisthesis, spondylolysis, spine biomechanics*

1. Introduction

Lumbar spondylolisthesis is defined as a spinal defect that causes the affected vertebra to be displaced anteriorly relative to the caudal vertebra [6], [17], [23]. This "slip" typically arises as a result of a failed locking mechanism and may remain static or progress over time [14]. Severity of spondylolisthesis can be graded 1 through 5. Grade 1 displacement of 0% to 25%, while grade 5 displacement is more than 100% [9]. Because of the mechanical instability, lumbar spondylolisthesis can be accompanied with low back pain, radicular lower limb pain and neurogenic claudication and is usually associated with disc degeneration [17], [23].

Spondylolisthesis is considered to have two main etiologies, spondylolytic and degenerative, both of which may share the same spinal disorder, but different pathogenesis [6]. Spondylolytic (isthmic) spondylolisthesis occurs due to osseous fracture (spondylolytic can be unilateral or bilateral) or elongation of the vertebral arch at the pars interarticularis [34]. In contrast, degenerative spondylolisthesis occurs due to degenerative changes in the spinal facet joints rather than a fracture [21]. Facet joints play an essential role in stabilizing

* Corresponding author: Suhaib Yaroub, Department of Biomedical Engineering, College of Engineering, Al-Nahrain University, Baghdad, Iraq. Phone: +9647707827789, e-mail: suhaib.yaroub@eng.nahrainuniv.edu.iq
Received: April 5th, 2022
Accepted for publication: June 30th, 2022

the segmental spine unit and slippage occurs when the locking mechanism fails [40]. The spinal level L4–L5 is the most commonly affected in degenerative spondylolisthesis and the second most commonly affected in isthmic spondylolisthesis [17], [40]. Understanding its biomechanics is critical for clinical prediction and therapy improvement.

Formerly, finite element (FE) models have been employed to investigate the biomechanics of spondylolysis and spondylolisthesis in the lumbar spine [7], [11], [16], [41]. Wang et al. [37] analyzed the biomechanics of the L5–S1 spine with high-grade spondylolisthesis after spinal fusion in a balanced and unbalanced pelvis [37]. Ramakrishna et al. [28] and Chen et al. [4] investigated the significance of sacral slope in the advancement of an L5 bilateral spondylolytic defect to spondylolisthesis and on the loading of pedicle screws in post-operative isthmic spondylolisthesis [4], [27]. Ramakrishna et al. [27] examined the impact of different grades of disc degeneration in the development of a bilateral L5-lytic defect to spondylolisthesis. Sterba et al. [35] performed a biomechanical analysis of spondylolysis with different intrinsic (spinopelvic postural) and extrinsic (loading conditions related to sports activities) parameters. To our knowledge, no biomechanical FE studies have been conducted to evaluate the effect of spondylolysis and spondylolisthesis on the kinematics of the L4–L5 lumbar spine.

In this research, nonlinear FE models were prepared from computed tomography (CT) images of a detailed educational L4–L5 spinal model to create a 3-dimensional model of the L4–L5 functional spinal unit (FSU) in an attempt to study the influence of spondylolysis and different form of grade 1 spondylolisthesis on the range of motion of the FSU from a biomechanical standpoint. In addition, the same models were modified to simulate the degenerative disc disease (DDD) for comparison. The clinical implication for this study was to determine the mechanical changes results from the above mentioned medical conditions and which movement might cause the progression to higher grade of spondylolisthesis in its different forms.

2. Materials and methods

Five nonlinear three-dimensional FE models were developed based on five realistic educational L4–L5 spine models obtained from Dynamic Disc Designs Corp. as listed:

- intact L4–L5 FSU dynamic disc model (INT);
- bilateral (isthmic) spondylolytic spondylolisthesis dynamic disc model (SPONDY);
- unilateral (right) pars defect spondylolytic spondylolisthesis dynamic disc Model (UNI);
- elongated pars spondylolisthesis dynamic disc model (LONG);
- degenerative spondylolisthesis dynamic disc model (DEGEN).

CT scans were used with 0.8 mm thickness (increment: 0.4 mm) for the above-mentioned models to get the geometric information.

The detailed steps for building and validating the FE model were obtained from previous research and briefly summarized here [1]. To reconstruct vertebral models, the software 3D Slicer (version: 4.13.0) was used to build surface models from DICOM (digital imaging and communications in medicine) images. The surface models were imported to SpaceClaim software (SpaceClaim 2020 R1, ANSYS, Inc) and reverse engineered to form a solid model and transferred to FE analysis software where the simulation took place. The validation process was done by replicating the testing setup and comparing the RoMs results of the intact model in the 3 orthogonal directions with published *in vitro* and *in silico* studies [2], [12], [13], [29], [30], [32], [38], [39].

All the models consisted of the following parts: vertebrae, intervertebral discs, endplates and ligaments, as shown in Fig. 1. The vertebrae consisted of the vertebral body (cortical and cancellous bones) and the posterior vertebral arch. The thickness of the cortical bone was assumed to be 0.6 mm [25]. The intervertebral disc (IVD) was divided into annulus fibrosus (AF) and nucleus pulposus (NP). The NP volume was set to 44% of the total disc volume and located 1.5 mm posterior to the center of the disc [19], [20], [24]. In addition, superior and inferior endplates were modeled between the IVD and both vertebral bodies. A total of 5 ligaments, including the anterior longitudinal ligament (ALL), posterior longitudinal ligament (PLL), ligamentum flavum (LF), interspinous ligament (ISL) and supraspinal ligament (SSL), were modeled as 3D elements and only used when subjected to tension load (PLL, LF, ISL, and SSL in flexion, ALL and SSL in extension, SSL in lateral bending, and no ligament in axial rotation) [12].

The material and geometric parameters for different parts of the model were obtained from the literature and summarized in Table 1 [10], [15], [18], [33], [39]. Both the anterior and posterior vertebral parts were modeled as a linear elastic material [10], [15], [18]. The AF and NP of the IVD were modeled using

a nonlinear hyperelastic material called the Mooney–Rivlin model and the nucleus was assumed to be nearly incompressible [10], [15], [18], [33], [39]. The ligaments were modeled as multi-linear mechanical properties [18]. The multi-linear material properties utilize more than two lines to describe the stress–strain relation. Based on the ligament strain value, different modulus of elasticity was implemented as displayed in Table 1. The contacts between all model elements were set as a binding connection. Facet joints were modeled with a frictionless contact interface.

Table 1. Material properties and geometrical parameters used in FE analysis

		Element type	Young's modules [MPa]	Poisson ratio	Element size [mm]	Area [mm^2]	References
Cortical bone		Isotropic, elastic	12000	0.3	1.0	–	[10], [15], [18]
Cancellous bone			100	0.2	2.0		
Posterior bone			3500	0.25	1.5		[10], [15]
Endplate			24	0.4	1.0		[10], [39]
AF	Flexion-extension	Mooney–Rivlin	C10 0.18; C01 0.045; D 1		0.5		[15], [18], [33]
	Bending and rotation		C10 0.56; C01 0.14; D 1				[10], [39]
NP	Flexion-extension, bending, and rotation	Mooney–Rivlin	C10 0.12; C01 0.03; D 1		1.0		[15], [18], [33]
ALL		Multi linear	347 ($\varepsilon < 12.2$) 787 ($12.2 < \varepsilon < 20.3$) 1864 ($20.3 < \varepsilon$)	0.3	1.5	63.7	[15], [18]
PLL			29.5 ($\varepsilon < 11.1$) 61.7 ($11.1 < \varepsilon < 23$) 236 ($23 < \varepsilon$)			20	
LF			7.7 ($\varepsilon < 5.9$) 9.6 ($5.9 < \varepsilon < 49$) 58.2 ($49 < \varepsilon$)			40	
ISL			1.4 ($\varepsilon < 13.9$) 1.5 ($13.9 < \varepsilon < 20$) 14.7($20 < \varepsilon$)			40	
SSL			2.5 ($\varepsilon < 20$) 5.3 ($20 < \varepsilon < 25$) 34 ($25 < \varepsilon$)			30	

Table 2. The changes in geometric information and material properties of IVD as a result of DDD

	Healthy Disc IVDH [mm]	DDD IVDH [mm]	DDD Material Properties [31]
INT	(A) 11.5 (C) 10.13 (P) 9.66	(A) 7.75 (C) 5.07 (P) 4.83	AF: Mooney–Rivlin C10 (MPa): 0.9; C01 (MPa): 0.23; D (1/MPa): 1 NP: Isotropic, elastic Young's modules (MPa): 1.66; Poisson ratio: 0.4
SPONDY	(A) 11.25 (C) 9.66 (P) 9.21	(A) 5.63 (C) 4.83 (P) 4.61	
LONG	(A) 10 (C) 7.614 (P) 7.136	(A) 5 (C) 3.81 (P) 3.57	
UNI	(A) 10.92 (C) 8.851 (P) 7.23	(A) 5.46 (C) 4.43 (P) 3.62	
DEGEN	NA	(A) 3.59 (C) 5.23 (P) 3.2	

IVDH: intervertebral disc height, (A) anterior, (C) central, (P) posterior.

Degenerative disc disease simulation

The models with healthy IVD were modified to simulate a moderate DDD at the L4-L5 lumbar level. DDD was simulated by decreasing the disc height and nucleus area and by modifying the material properties of the AF and NP (Table 2). Disc height collapse was modeled as a 50% reduction in disc height measured in the mid-sagittal plane by moving the L4 inferiorly while maintaining the L4–L5 facet articulation [28]. A 40% expansion of the annulus volume was achieved by decreasing the NP volume to maintain the same disc volume [5]. Furthermore, both the AF and NP strength were increased due to dehydration and the material properties for the degenerated disc were taken from the literature [31].

Loads and boundary constraints

In all the models, the inferior surface of L5 was kinematically constrained at six degrees of freedom. Moreover, a pure moment of 1, 2.5, 5, 7.5 and 10 Nm in three different orientations (flexion-extension, right lateral bending and right axial rotation) were applied to the superior surface of the L4 vertebral body.

All the model components were meshed with first-order tetrahedral elements. The element size for each part of the models were listed in Table 1. For each model used, the number of nodes and elements for all the movements were average and the final numbers were as follows: INT models (nodes: 183,740, elements: 830,752) for healthy disc and (nodes: 154,152, elements: 669,639) for DDD, SPONDY models (nodes: 175,450, elements: 777,064) for healthy disc and (nodes: 141,070, elements: 592,233) for DDD, UNI models (nodes: 163,731, elements: 714,779) for healthy disc and (nodes: 135,090, elements: 559,577) for DDD, LONG models (nodes: 164,775, elements: 720,761) for healthy disc and (nodes: 141,944, elements: 598,244) for DDD and DEGEN model (nodes: 152,663, elements: 638,548) for DDD. All the mesh manipulation and simulation work were conducted using FE analysis software (ANSYS 2020 R1, ANSYS, Inc.) and implemented into a laptop computer with an Intel Core i7-9750H CPU and 24Gb RAM.

3. Results

The present study obtained the RoMs under four loading conditions (including the flexion, extension, right lateral bending and right axial rotation) of five different FSUs with healthy and DDD IVD (9 FE models in total). INT model data were used as baseline values for describing the change in RoM in these FE models.

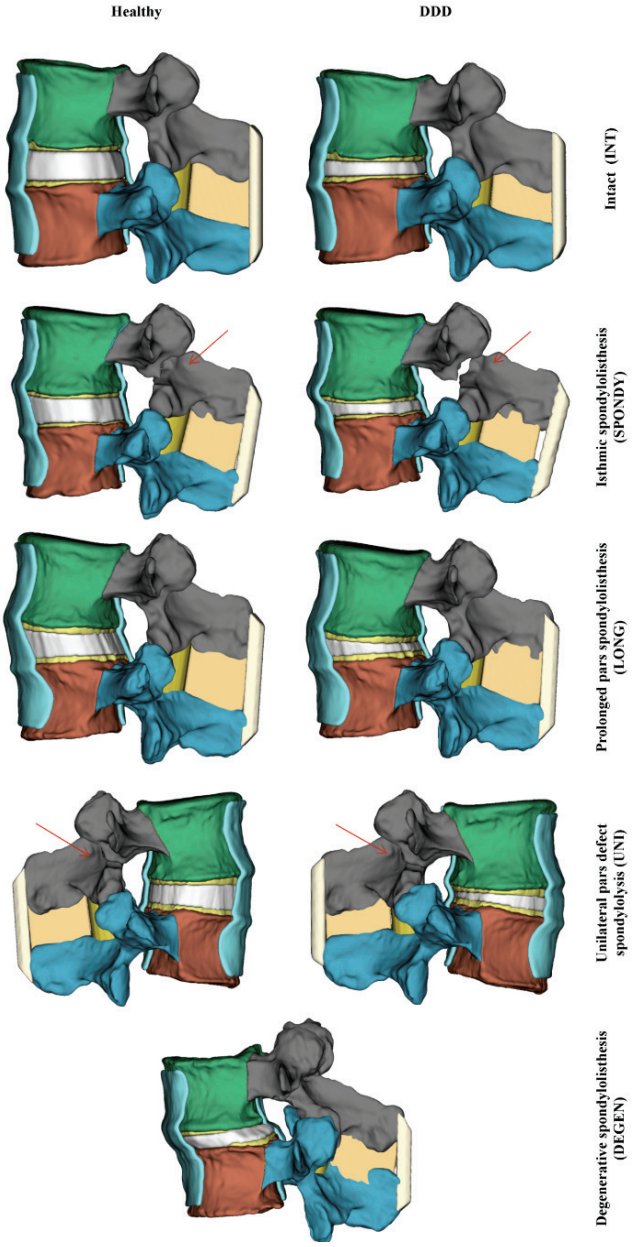

Fig. 1. A lateral view of the L4–L5 FSU 3D models used in this study. Red arrow indicates the site of the defect

The total RoMs of all FE models for applied moments of 10 Nm were presented in Fig. 2. In healthy IVD, in flexion-extension, the total rotation of 10.6°, 16.3°, 10.4°, and 9.5° was reached at 10 Nm applied moment for the INT, SPONDY, LONG and UNI, respectively. In the case of lateral bending loading and axial rotation, the angular rotations were (7.4°, 7.7°, 7.2°, and 7.2°) and (3°, 14.5°, 3.1°, and 5°) for INT, SPONDY, LONG, and UNI FE models, respectively.

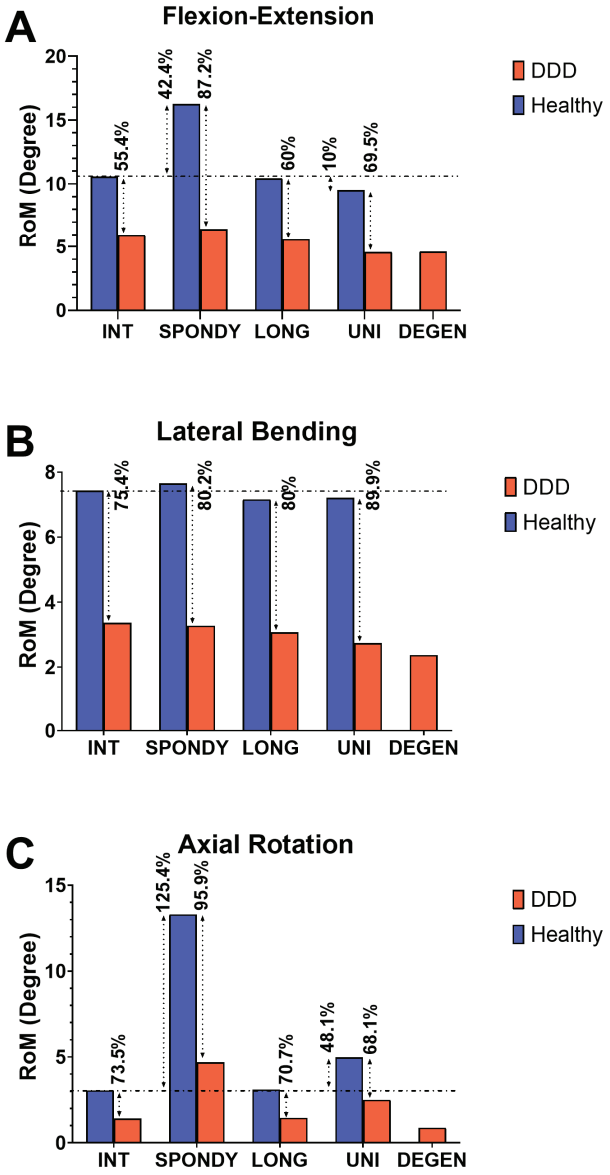

Fig. 2. Comparison of the RoMs between the FE models utilized in this study: (A) flexion-extension, (B) right lateral bending, (C) right axial rotation

The SPODNY produced an increase of RoM by 42.4%, whereas the LONG and UNI models had a decrease of 1.9% and 10%, respectively, compared to the INT model in flexion-extension. Under the lateral bending, an increase of 4% for the SPODNY model and a decrease of 1.67% for both LONG and UNI models were observed, whereas increases of 125.4%, 3.3%, and 48.1% were shown for SPONDY, LONG, and UNI models, respectively, during axial rotation.

The models with the DDD IVD exhibited a stiffer response than the healthy disc ones. In flexion-extension, a total rotation of 6, 6.4, 5.6, 4.6, and 4.6° was reached at 10 Nm applied moment for the INT, SPONDY, LONG, UNI, and DEGEN, respectively. In the case of lateral bending and axial rotation, the angular rotations were (3.4, 3.3, 3.1, 2.7, and 2.4°) and (1.4, 4.7, 1.5, 2.5, and 0.9°) for INT, SPONDY, LONG, UNI, and DEGEN FE models, respectively.

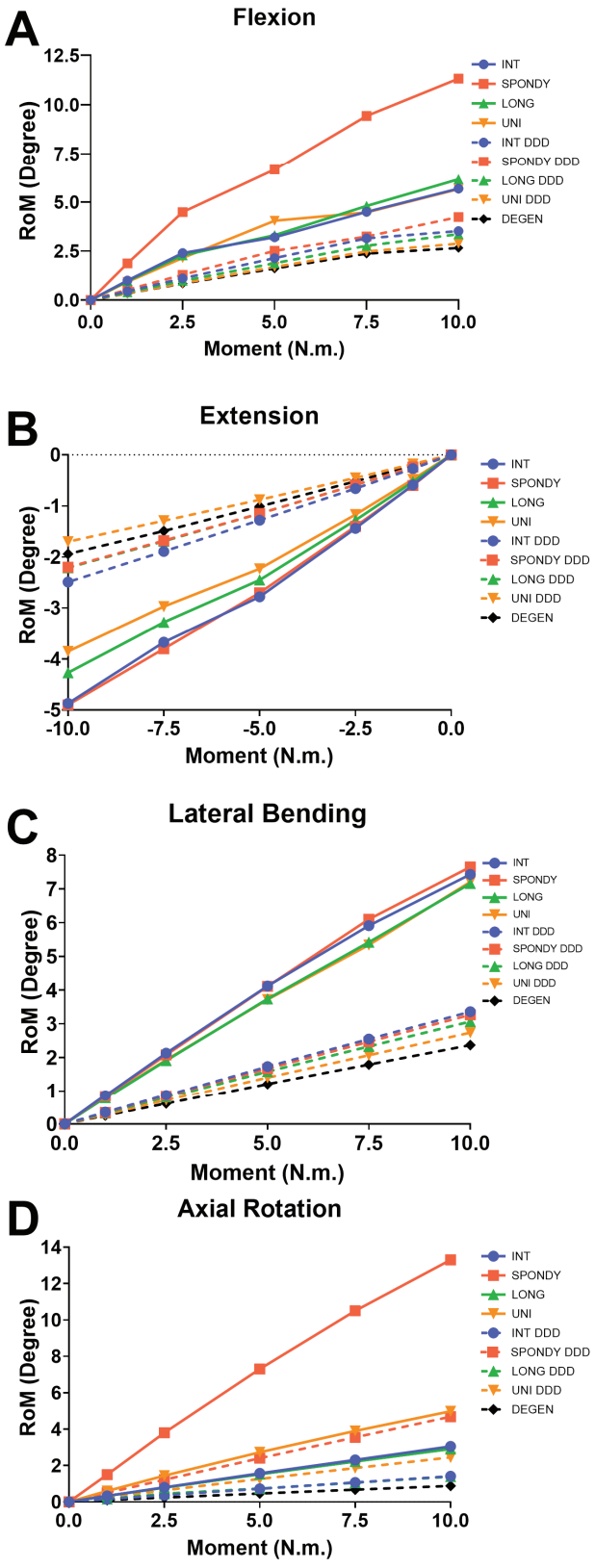

Fig. 3. RoM-moment curves of FE models in (A) flexion, (B) extension, (C) right lateral bending, (D) right axial rotation

In Figure 3, the angular displacement of all developed FE models in response to the applied moments (up to 10 Nm) and in 3 orthogonal planes are shown. Generally, a nonlinear behavior was noticed in the healthy disc models while with the DDD models, the response became stiffer and the motion patterns became more linear under the exact applied moment.

The rotation curves of the flexion movement between L4 and L5 vertebrae are shown in terms of the applied moment (Fig. 3A). Under flexion loading, the healthy disc SPONDY model displayed an enormous flexible response with 11.32° at 10 Nm whereas the LONG and UNI models with a healthy disc showed a comparable response of 6.17° and 5.66° at 10 Nm, respectively, to the healthy disc INT model (5.69° at 10 Nm). The models with the DDD IVD exhibited a stiffer response than the healthy ones. The DEGEN model displayed the stiffest response with a rotation of 2.66° at a 10 Nm applied moment. Moreover, rotations of 3.52°, 4.24°, 3.36°, and 2.88° were reached at the maximum applied moment for the INT, SPONDY, LONG, UNI models.

In the case of extension loading (Fig. 3B), the SPONDY model with a healthy disc has shown a moment-rotation relationship much more similar to that exhibited by the INT one (–4.9° vs. –4.87° at –10 Nm). However, stiffer responses (–4.27° and –3.85°) were noticed by the LONG and UNI models compared to the INT model at the exact applied moment. For the DDD models, the UNI model displayed the stiffest response with a rotation of –1.70° at –10 Nm applied moment and a rotation of –2.49°, –2.20°, –2.21°, and –1.94° were reached at the maximum applied moment for the INT, SPONDY, LONG, DEGEN models.

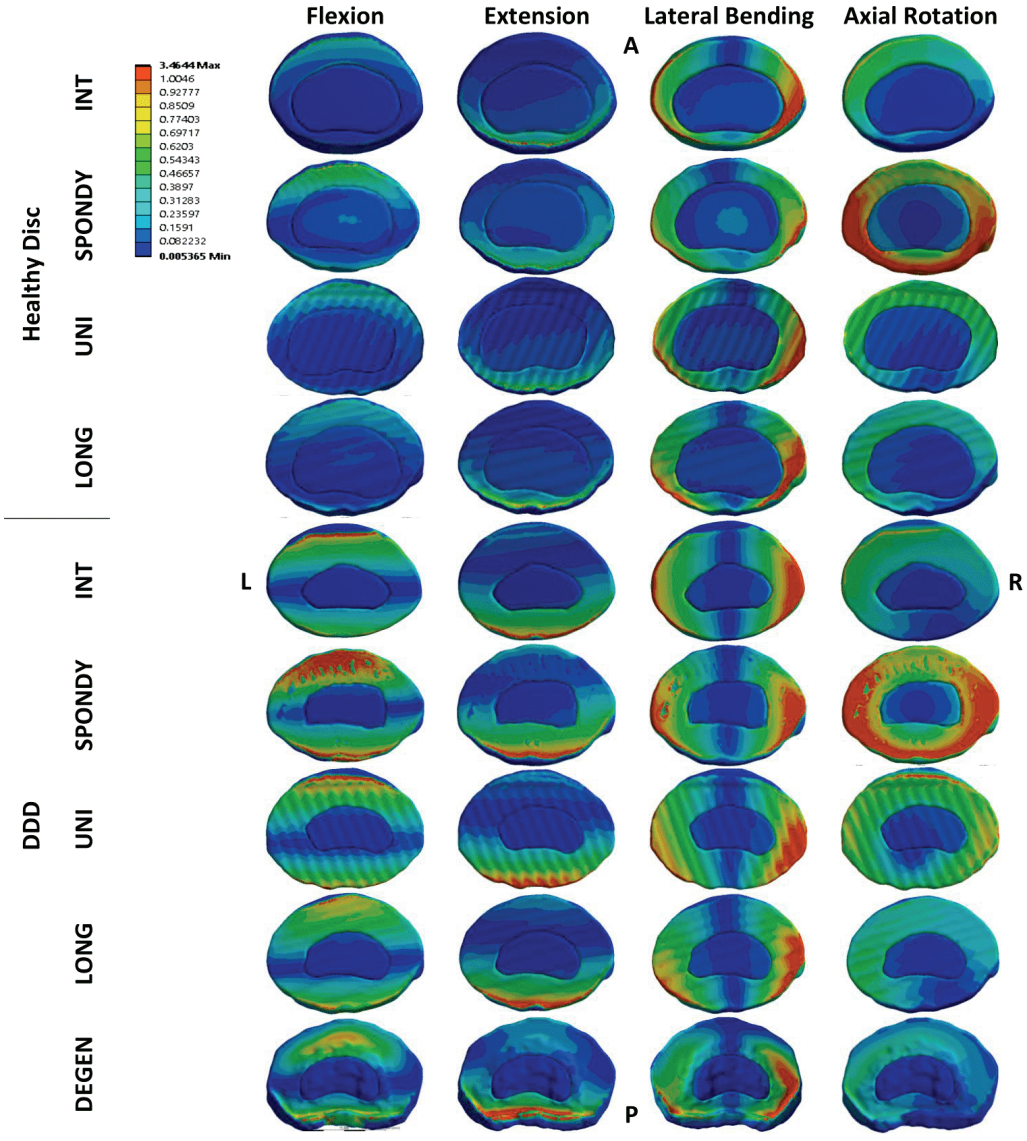

Fig. 4. Von Mises stress distribution [MPa] at the L4–L5 IVDs (healthy and DDD) for the INT, SPONDY, UNI, LONG, and DEGEN FE models in flexion, extension, lateral bending, and axial rotation

In Figure 3 C, the applied lateral bending moment versus the relative rotation between the two vertebrae L4 and L5 curves for all the considered cases are illustrated. In contrast to flexion, spondylosis and spondylolisthesis in the healthy disc models did not significantly affect the moment-rotation relationships and all cases exhibited a similar response. On the other hand, the same patterns (comparable results) but with stiffer responses were noticed in DDD models except for the DEGEN model, where the lowest angular rotation of 2.37° reached at 10 Nm lateral bending moment.

In the axial rotation case, the moment-rotation curves were presented in Fig. 3 D. The healthy disc SPONDY model displayed an enormous flexible response with 13.3° at 10 Nm. Also, the UNI model showed a flexible curve with a rotation of 4.98° at 10 Nm. In contrast, the healthy disc LONG model showed a comparable response of 2.91° at 10 Nm to the healthy disc INT model (3.05° at 10 Nm). In the DDD IVD case, both the SPONDY and UNI models exhibited a more flexible response than the INT one, with a rotation of 4.68° and 2.45° at 10 Nm, respectively. The DEGEN model displayed the stiffest response with a rotation of 0.88° at a 10 Nm applied moment. Moreover, a rotations of 1.41° and 1.39° were reached at the maximum applied moment for the INT and LONG DDD models.

A total of 72 (36 stress and 36 strain) colour coded Von Mises stresses and Von Mises strains distribution in the IVD of all the L4–L5 FSUs with healthy and DDD discs during all 4 movements were presented in Figs. 4 and 5. All the results were analysed at peak of applied moment (10 Nm) in all the FE models. Both healthy and DDD models shared the same pattern in the stresses and strains distributions. However, the stress distributions in DDD models were higher in values compared to the healthy disc models while the opposite applies to strain maps. During flexion and axial rotation, the greatest increase in the stress and

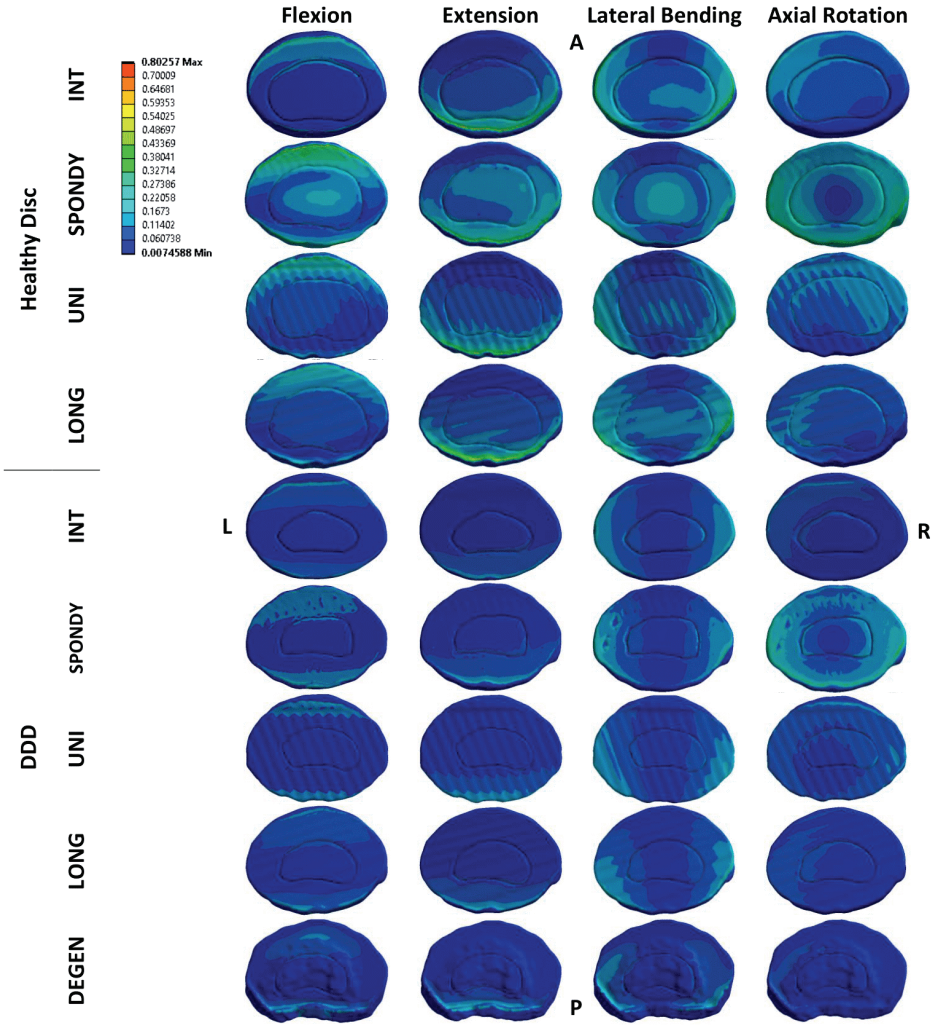

Fig. 5. Von Mises strain distribution at the L4−L5 IVDs (healthy and DDD)
for the INT, SPONDY, UNI, LONG and DEGEN FE models in flexion, extension, lateral bending and axial rotation

strain from the baseline INT state was observed in both SPONDY models while in extension and lateral bending, comparable results were noted in all the models.

4. Discussion

A better understanding of how spondylolysis and different types of grade 1 spondylolisthesis affects the kinematics of the L4–L5 lumbar spine segment with healthy and DDD IVD may result in more informed decisions about its treatment and postsurgical complications. The focus of this study was to evaluate and characterize lumbar segmental motion using the FE method. In general, the results showed that the models could give detailed quantitative information on the mechanical behavior of the spine with the above-mentioned medical conditions.

The results indicate that the isthmic spondylolisthesis appears to alter the normal movement of the affected level the most in both flexion and axial rotation. Increases of 66.2% and 125.4% in the RoMs in both flexion and axial rotation, respectively, were measured from the isthmic spondylolisthesis with the healthy IVD model compared to the INT model. Similarly, the same pattern was noticed (18.6% in flexion and 107.4% in axial rotation) with the DDD models. This motion instability is due to the loss of the SSL, ISL and LF effect due to the separation of the anterior part of the L4 vertebra from the posterior part and the anterior displacement. These observations support the published experimental and FE findings showing a bilateral lytic defect in the lumbar spine greatly enhances segmental mobility [3], [8], [11], [27], [36].

However, the results of spondylolysis with unilateral pars defect reveal a significant increase in axial rotation in both healthy and DDD disc models (48.1% and 53.9%, respectively). This increase in motion increases the stress in the contralateral pars interarticularis, which eventually leads to bilateral pars defect. A comparison between the INT, LONG and UNI revealed that both LONG and UNI exhibit a slightly stiffer behavior in extension. Differences of 13.1% and 23.4% for the LONG and UNI models, respectively, were measured compared to the INT model. Likewise, the LONG and UNI DDD models have a difference of 11.9% and 37.7%, respectively, compared to the INT model.

The results presented in Fig. 3 show a grade 1 slip at the L4–L5 segment resulting from degenerative spondylolisthesis displaying the largest decrease in angular motion of the lumbar spine. This motion reduction is due to the changes in the facet joints and the considerable reduction in disc height. These findings support prior studies that demonstrated lumbar spine hypomobility in the presence of degenerative spondylolisthesis [22], [26].

Comparing the results obtained from the DDD models with the healthy disc models, it can be noted that the RoMs curves in flexion, extension, lateral bending and axial rotation of the DDD FE models were showing the same pattern but with lower values compared to the healthy disc ones. As shown in Fig. 2, the largest variation in flexion-extension between the healthy and DDD models can be noted in the SPONDY models (87.2%) while in lateral bending, all models share comparable results of the RoM variation between the healthy and DDD discs with the UNI models having the highest variation (89.9%). In axial rotation, similar to the flexion-extension, the SPONDY models had the largest RoM variation of (95.9%). These results are comparable to the published studies [27].

This study has several limitations that should be mentioned. First, the geometric variation of the vertebra, such as the vertebral shape and size, disc height and lordosis angle, were not considered in the study, and only the geometries of educational models were used. Next, the loading conditions used in this study were simple and did not replicate the actual loading condition acting on the lumbar spine inside the body (such as body weight and muscle forces). Additionally, we evaluated the FE models of a single vertebral segment. However, a multiple-segment provides a more accurate picture of the clinical situation. Last, only a 50% collapse in disc height was modeled.

Nevertheless, the developed models described the kinematics of the medical condition studied in this research and can be used as a starting point for more complex scenarios and loading conditions to further exam the cause of progression of the grade 1 spondylolisthesis to a higher grade of spondylolisthesis in its different forms.

5. Conclusions

In conclusion, the biomechanical behavior of spondylotic and different types of grade 1 spondylolisthesis of the L4–L5 FSU has been demonstrated in this study and compared with the intact model. The results show that in isthmic spondylolisthesis, hypermobility was noticed in both flexion and axial rotation. In compari-

son, degenerative spondylolisthesis with severe disc degeneration displays a high hypomobility of the L4–L5 spinal segment. Lastly, the unilateral spondylolysis L4 defect displays hypermobility in axial rotation and the prolonged pars spondylolisthesis does not significantly impact the spinal segment range of motion.

Acknowledgements

The authors would like to thank Buratha Diagnostic Center for help in acquiring the CT scan used in this study.

References

[1] AL-RUBAIE S.Y., HAMANDI S.J., MOHSON K.I., *Kinematic validation of an intact L4–L5 spinal unit finite element model constructed from an educational model*, Int. J. Mech. Eng., 2022, 7 (2).

[2] BASHKUEV M., REITMAIER S., SCHMIDT H., *Is the sheep a suitable model to study the mechanical alterations of disc degeneration in humans? A probabilistic finite element model study*, J. Biomech., 2019, 84, DOI: 10.1016/J.JBIOMECH.2018.12.042.

[3] CHAMOLI U., CHEN A.S., DIWAN A.D., *Interpedicular kinematics in an in vitro biomechanical assessment of a bilateral lumbar spondylolytic defect*, Clin. Biomech., 2014, 29 (10), DOI: 10.1016/J.CLINBIOMECH.2014.10.002.

[4] CHEN L., FENG Y., CHE C.Q., GU Y., WANG L.J., YANG H.L., *Influence of Sacral Slope on the Loading of Pedicle Screws in Postoperative L5/S1 Isthmic Spondylolisthesis Patient: A Finite Element Analysis*, Spine, 2016, 41 (23), DOI: 10.1097/BRS.0000000000001632.

[5] CHUANG W.H., KUO Y.J., LIN S.C., WANG C.W., CHEN S.H., CHEN Y.J., HWANG J.R., *Comparison among load-, ROM-, and displacement-controlled methods used in the lumbosacral nonlinear finite-element analysis*, Spine, 2013, 38 (5), DOI: 10.1097/BRS.0B013E31828251F9.

[6] DENARD P.J., HOLTON K.F., MILLER J., FINK H.A., KADO D.M., YOO J.U., MARSHALL L.M., *Lumbar spondylolisthesis among elderly men: prevalence, correlates, and progression*, Spine, 2010, 35 (10), DOI: 10.1097/BRS.0b013e3181bd9e19.

[7] EL-RICH M., VILLEMURE I., LABELLE H., AUBIN C.E., *Mechanical loading effects on isthmic spondylolytic lumbar segment: finite element modelling using a personalised geometry*, Comput. Methods Biomech. Biomed. Engin., 2009, 12 (1), DOI: 10.1080/10255840802069823.

[8] FAN J., YU G.R., LIU F., ZHAO J., ZHAO W.D., *A biomechanical study on the direct repair of spondylolysis by different techniques of fixation*, Orthop. Surg., 2010, 2 (1), DOI: 10.1111/J.1757-7861.2009.00064.X.

[9] GARET M., REIMAN M.P., MATHERS J., SYLVAIN J., *Nonoperative Treatment in Lumbar Spondylolysis and Spondylolisthesis: A Systematic Review*, Sports Health, 2013, 5 (3), DOI: 10.1177/1941738113480936.

[10] HADDAS R., XU M., LIEBERMAN I., YANG J., *Finite Element Based-Analysis for Pre and Post Lumbar Fusion of Adult Degenerative Scoliosis Patients*, Spine Deform, 2019, 7 (4), DOI: 10.1016/J.JSPD.2018.11.008.

[11] HAJ-ALI R., WOLFSON R., MASHARAWI Y., *A patient specific computational biomechanical model for the entire lumbosacral spinal unit with imposed spondylolysis*, Clin. Biomech., 2019, 68, DOI: 10.1016/J.CLINBIOMECH.2019.05.022.

[12] HEUER F., SCHMIDT H., KLEZL Z., CLAES L., WILKE H.J., *Stepwise reduction of functional spinal structures increase range of motion and change lordosis angle*, J. Biomech., 2007, 40 (2), DOI: 10.1016/J.JBIOMECH.2006.01.007.

[13] JARAMILLO H.E., GÓMEZ L., GARCÍA J.J., *A finite element model of the L4-L5-S1 human spine segment including the heterogeneity and anisotropy of the discs*, Acta Bioeng. Biomech., 2015, 17 (2), DOI: 10.5277/ ABB-00046-2014-02.

[14] JAYAKUMAR P., NNADI C., SAIFUDDIN A., MACSWEENEY E., CASEY A., *Dynamic degenerative lumbar spondylolisthesis: diagnosis with axial loaded magnetic resonance imaging*, Spine, 2006, 31 (10), DOI: 10.1097/01.BRS.0000216602.98524.07.

[15] JIANG S., LI W., *Biomechanical study of proximal adjacent segment degeneration after posterior lumbar interbody fusion and fixation: a finite element analysis*, J. Orthop. Surg. Res., 2019, 14 (1), DOI: 10.1186/S13018-019-1150-9.

[16] JOSZKO K., GZIK M., WOLAŃSKI W., GZIK-ZROSKA B., KAWLEWSKA E., *Biomechanical evaluation of human lumbar spine in spondylolisthesis*, J. Appl. Biomed., 2018, 16 (1), DOI: 10.1016/J.JAB.2017.10.004.

[17] KHAN S.A., SATTAR A., KHANZADA U., ADEL H., ADIL S.O., HUSSAIN M., *Facture of the Pars Interarticularis with or without Spondylolisthesis in an Adult Population in a Developing Country: Evaluation by Multidetector Computed Tomography*, Asian Spine J., 2017, 11 (3), DOI: 10.4184/ASJ.2017.11.3.437.

[18] LING Q., HE E., ZHANG H., LIN H., HUANG W., *A novel narrow surface cage for full endoscopic oblique lateral lumbar interbody fusion: A finite element study*, J. Orthop. Sci., 2019, 24 (6), DOI: 10.1016/J.JOS.2019.08.013.

[19] LIU T., EL-RICH M., *Effects of nucleus pulposus location on spinal loads and joint centers of rotation and reaction during forward flexion: A combined finite element and Musculoskeletal study*, J. Biomech., 2020, 104, DOI: 10.1016/J.JBIOMECH.2020.109740.

[20] MASNI-AZIAN, TANAKA M., *Biomechanical investigation on the influence of the regional material degeneration of an intervertebral disc in a lower lumbar spinal unit: A finite element study*, Comput. Biol. Med., 2018, 98, DOI: 10.1016/J.COMPBIOMED.2018.05.010.

[21] MATSUNAGA S., IJIRI K., HAYASHI K., *Nonsurgically managed patients with degenerative spondylolisthesis: a 10- to 18-year follow-up study*, J. Neurosurg., 2000, 93 (2), DOI: 10.3171/SPI.2000.93.2.0194.

[22] MCGREGOR A.H., CATTERMOLE H.R., HUGHES S.P.F., *Global spinal motion in subjects with lumbar spondylolysis and spondylolisthesis: does the grade or type of slip affect global spinal motion?*, Spine, 2001, 26 (3), DOI: 10.1097/00007632-200102010-00013.

[23] MIAO J., WANG S., WAN Z., PARK W.M., XIA Q., WOOD K., LI G., *Motion characteristics of the vertebral segments with lumbar degenerative spondylolisthesis in elderly patients*, Eur. Spine J., 2013, 22 (2), DOI: 10.1007/s00586-012-2428-3.

[24] NASERKHAKI S., ARJMAND N., SHIRAZI-ADL A., FARAHMAND F., EL-RICH M., *Effects of eight different ligament property datasets on biomechanics of a lumbar L4-L5 finite element model*, J. Biomech., 2018, 70, DOI: 10.1016/J.JBIOMECH.2017.05.003.

[25] PENG Y., DU X., HUANG L., LI J., ZHAN R., WANG W., XU B., WU S., PENG C., CHEN S., *Optimizing bone cement stiffness for vertebroplasty through biomechanical effects analysis based on patient-specific three-dimensional finite element modeling*, Med. Biol. Eng. Comput., 2018, 56 (11), DOI: 10.1007/S11517-018-1844-X.

[26] PHAN K.H., DAUBS M.D., KUPPERMAN A.I., SCOTT T.P., WANG J.C., *Kinematic analysis of diseased and adjacent segments in degenerative lumbar spondylolisthesis*, Spine J., 2015, 15 (2), DOI: 10.1016/J.SPINEE.2014.08.453.

[27] RAMAKRISHNA V.A.S., CHAMOLI U., VIGLIONE L.L., TSAFNAT N., DIWAN A.D., *Mild (not severe) disc degeneration is implicated in the progression of bilateral L5 spondylolysis to spondylolisthesis*, BMC Musculoskelet. Disord., 2018, 19 (1), DOI: 10.1186/S12891-018-2011-0.

[28] RAMAKRISHNA V.A.S., CHAMOLI U., VIGLIONE L.L., TSAFNAT N., DIWAN A.D., *The Role of Sacral Slope in the Progression of a Bilateral Spondylolytic Defect at L5 to Spondylolisthesis: A Biomechanical Investigation Using Finite Element Analysis*, Glob Spine J., 2018, 8 (5), DOI: 10.1177/2192568217735802.

[29] REMUS R., LIPPHAUS A., NEUMANN M., BENDER B., *Calibration and validation of a novel hybrid model of the lumbosacral spine in ArtiSynth-The passive structures*, PLoS One, 2021, 16 (4), DOI: 10.1371/JOURNAL.PONE.0250456.

[30] ROHLMANN A., ZANDER T., SCHMIDT H., WILKE H.J., BERGMANN G., *Analysis of the influence of disc degeneration on the mechanical behaviour of a lumbar motion segment using the finite element method*, J. Biomech., 2006, 39 (13), DOI: 10.1016/J.JBIOMECH.2005.07.026.

[31] RUBERTÉ L.M., NATARAJAN R.N., ANDERSSON G.B., *Influence of single-level lumbar degenerative disc disease on the behavior of the adjacent segments-a finite element model study*, J. Biomech., 2009, 42 (3), DOI: 10.1016/J.JBIOMECH.2008.11.024.

[32] SCHMIDT H., GALBUSERA F., ROHLMANN A., ZANDER T., WILKE H.J., *Effect of multilevel lumbar disc arthroplasty on spine kinematics and facet joint loads in flexion and extension: a finite element analysis*, Eur. Spine J., 2012, 21, DOI: 10.1007/S00586-010-1382-1.

[33] SCHMIDT H., HEUER F., DRUMM J., KLEZL Z., CLAES L., WILKE H.J., *Application of a calibration method provides more realistic results for a finite element model of a lumbar spinal segment*, Clin. Biomech., 2007, 22 (4), DOI: 10.1016/J.CLINBIOMECH.2006.11.008.

[34] SPIVAK J.M., KUMMER F.J., CHEN D., QUIRNO M., KAMERLINK J.R., *Intervertebral foramen size and volume changes in low grade, low dysplasia isthmic spondylolisthesis*, Spine, 2010, 35 (20), DOI: 10.1097/BRS.0B013E3181CCC59D.

[35] STERBA M., ARNOUX P.J., LABELLE H., WARNER W.C., AUBIN C.É., *Biomechanical analysis of spino-pelvic postural configurations in spondylolysis subjected to various sport-related dynamic loading conditions*, Eur. Spine J., 2018, 27 (8), DOI: 10.1007/S00586-018-5667-0.

[36] WANG J.P., ZHONG Z.C., CHENG C.K., CHEN C.S., YU C.H., CHANG T.K., WEI S.H., *Finite element analysis of the spondylolysis in lumbar spine*, Biomed. Mater Eng., 2006, 16 (5).

[37] WANG W., AUBIN C.E., CAHILL P., BARAN G., ARNOUX P.J., PARENT S., LABELLE H., *Biomechanics of high-grade spondylolisthesis with and without reduction*, Med. Biol. Eng. Comput., 2016, 54 (4), DOI: 10.1007/S11517-015-1353-0.

[38] WEISSE B., AIYANGAR A.K., AFFOLTER C., GANDER R., TERRASI G.P., PLOEG H., *Determination of the translational and rotational stiffnesses of an L4–L5 functional spinal unit using a specimen-specific finite element model*, J. Mech. Behav. Biomed. Mater, 2012, 13, DOI: 10.1016/J.JMBBM.2012.04.002.

[39] XIAO Z., WANG L., GONG H., ZHU D., ZHANG X., *A non-linear finite element model of human L4–L5 lumbar spinal segment with three-dimensional solid element ligaments*, Theor. Appl. Mech. Lett., 2011, 1 (6), DOI: 10.1063/2.1106401.

[40] YAO Q., WANG S., SHIN J.H., LI G., WOOD K.B., *Lumbar Facet Joint Motion in Patients with Degenerative Spondylolisthesis*, J. Spinal Disord. Tech., 2013, 26 (1), DOI: 10.1097/BSD.0B013E31827A254F.

[41] ZHU R., NIU W.X., ZENG Z.L., TONG J.H., ZHEN Z.W., ZHOU S., YU Y., CHENG L.M., *The effects of muscle weakness on degenerative spondylolisthesis: A finite element study*, Clin. Biomech., 2017, 41, DOI: 10.1016/J.CLINBIOMECH.2016.11.007.